

Galaxies at $z \approx 4$ and the Formation of Population II¹

S. C. Trager², S. M. Faber

UCO/Lick Observatory and Board of Studies in Astronomy and Astrophysics, University of California, Santa Cruz

Alan Dressler & Augustus Oemler, Jr.

Observatories of the Carnegie Institution of Washington

ABSTRACT

We report the discovery of four high-redshift objects ($3.3 < z < 4$) observed behind the rich cluster CL0939+4713 (Abell 851). One object (DG 433) has a redshift of $z = 3.3453$; the other three objects have redshifts of $z \approx 4$: A0 at $z = 3.9819$, DG 353 and P1/P2 at $z = 3.9822$. It is possible that all four objects are being lensed in some way by the cluster, DG 433 being weakly sheared, A0 being strongly sheared, and DG 353 and P1/P2 being an image pair of a common source object; detailed modelling of the cluster potential will be necessary to confirm this hypothesis. The weakness of common stellar wind features like N V and especially C IV in the spectra of these objects argues for sub-solar metallicities, at least as low as the SMC. DG 353 and DG 433, which have ground-based colors, are moderately dusty [$E_{\text{int}}(B - V) \lesssim 0.15$], similar to other $z > 3$ galaxies. Star formation rates range from $2.5 (7.8) h^{-2}$ to $22. (78.) h^{-2} M_{\odot} \text{ yr}^{-1}$, for $q_0 = 0.5 (0.05)$, depending on assumptions about gravitational lensing and extinction, also typical of other $z > 3$ galaxies. These objects are tentatively identified as the low-metallicity proto-spheroid clumps that will merge to form the Population II components of today's spheroids.

Subject headings: galaxies: formation — galaxies: clusters: individual (CL0939+4713)
— gravitational lensing

1. Introduction

Identifying the precursors of today's old stellar populations—ellipticals and bulges of spirals—is one of the major goals of observational cosmology. Until recently, we have been confined

¹Based on observations taken with the NASA/ESA *Hubble Space Telescope* obtained at the Space Telescope Science Institute, which is operated by AURA under NASA contract NAS5-26555, and observations obtained at the W. M. Keck Observatory, which is operated jointly by the University of California and the California Institute of Technology

²Present address: Observatories of the Carnegie Institution of Washington, 813 Santa Barbara Street, Pasadena, CA 91101

to studying either galaxies at lookback times of less than half a Hubble time or extremely distant, luminous objects such as radio galaxies or QSOs. With the advent of 8–10m class telescopes, faint star-forming galaxies at $2.5 > z > 4.5$ are now accessible. Steidel et al. (1996a, 1996b; Giavalisco, Steidel, & Macchetto 1996) have pioneered a multicolor technique to select candidates by use of color “dropouts.” At least 17 objects at $z > 2.5$ have been found in the Hubble Deep Field using this technique as of this writing (Steidel et al. 1996b; Lowenthal et al. 1997). Other groups have had success searching for QSO companions (Malkan, Teplitz & McLean 1996; Hu & McMahon 1996; Hu, McMahon, & Egami 1996; Petitjean et al. 1996) or using gravitational lensing to improve detectability (Ebbels et al. 1996). Some high-redshift objects have been discovered serendipitously in deep redshift surveys (Yee et al. 1996, Ellingson et al. 1996).

In this paper we report observations of four high-redshift objects ($3.3 < z < 4$) observed through the intermediate-redshift cluster CL0939+4713 (Abell 851, $z \approx 0.4$). These objects were discovered serendipitously during a program to study the stellar populations of early-type galaxies in this cluster. CL0939+4713 has been the subject of intensive study over the past 15 years (Dressler & Gunn 1992; Dressler et al. 1993, 1994a,b; Moore et al. 1996; Trager 1997) as an excellent laboratory for studying the evolutionary state of galaxies at $z = 0.41$. It has also been the subject of a weak-field gravitational lensing study by Seitz et al. (1996), who identified three of our four objects as candidate lensed galaxies.

We use the properties of our newly discovered objects, together with those of other high-redshift samples, to argue that high-redshift galaxies are metal-poor subclumps that will merge to form the Population II components of today’s spheroids.

2. Observations

The observations were taken as part of a multislit spectral survey of objects in CL0939+4713 and the superposed field. Two faint, morphologically peculiar objects (DG 353, DG 433; Dressler & Gunn 1992) were selected near the core of the cluster from the HST images of Dressler et al. (1994b), Figure 1, to sample what we then believed to be dwarf irregular cluster members. These and about twenty other objects were observed through a multi-aperture plate with the LRIS spectrograph (Oke et al. 1995) for 7200 s on 18 March 1995. The plates were punched with slit widths of 0.7 arcsecond. The seeing was $0''.7$ FWHM, the instrumental resolution was $\approx 7.5 \text{ \AA}$, and the spectral range was 3700–9000 \AA .

While preparing for a second Keck run in March 1996, we reduced and re-examined these spectra in early February 1996 using the EXPECTOR spectral extraction package (Kelson et al. 1997). The spectra of DG 353 and DG 433 proved not to be those of dwarf galaxies at $z \approx 0.4$; rather, they resembled the spectra of high-redshift ($z > 3$) star-forming galaxies discovered by Steidel et al. (1996a).

Based on these results, we selected several more faint, morphologically peculiar objects.

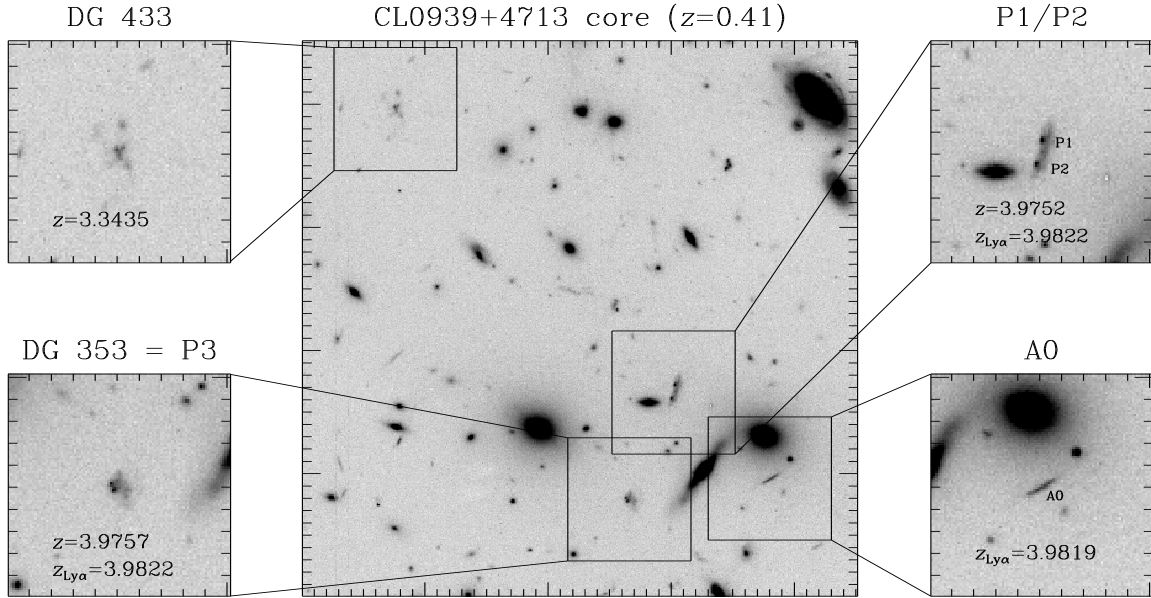


Fig. 1.— The core of CL0939+4713 as imaged by the *Hubble Space Telescope*. The bright galaxies are cluster members at $z = 0.41$; the fainter galaxies are a combination of faint dwarf galaxies in the cluster and very distant galaxies behind the cluster. The central panel is $140 h^{-1}$ kpc on a side at the distance of the cluster. The four side panels are expanded views of four very distant galaxies behind the cluster. Each panel is about $30 h^{-1}$ kpc across in the rest frame of the objects (assuming no lensing), and the resolution is about $0.3 h^{-1}$ kpc. North is to the top, east is to the left; the small ticks are $1''$ apart.

These included two arc-like objects recently suggested as possibly gravitationally lensed and distorted images of distant background galaxies (Seitz et al. 1996; these are P1/P2 and A0 in their notation, see Figure 1; in their notation, DG 353 is also known as P3). We used tilted slitlets on the multi-aperture plates to cover multiple objects (in the case of P1/P2) or to follow the major axis of the object (A0). The plate with a slitlet for P1/P2 was exposed for a total of 6382 s on 16 March 1996, and the plate with a slitlet for A0 was exposed for a total of 7200 s on 16–17 March 1996. The instrumental configuration was identical to the March 1995 run. The seeing was slightly worse and variable, ranging from $0''.7$ to $1''.1$. Reductions were again performed using the EXPECTOR spectral extraction package (Kelson et al. 1997).

Spectra of the four objects are shown in Figure 2. A sum of the four objects (below) is shown in the fifth panel, and a spectrum of NGC 1741B1, a knot in a nearby starburst galaxy (Conti, Leitherer & Vacca 1996), kindly provided by C. Leitherer, is shown in the sixth panel for comparison, redshifted and convolved to the resolution of the object spectra.

3. Results

3.1. Redshifts

Redshifts were measured independently for these objects from detected absorption lines and from Ly α emission (not detected in DG 433). These redshifts are summarized in Table 1.

We detect weak low-ionization interstellar absorption lines of Si II, C II, and possibly O I in three of these objects (DG 433, DG 353, and P1/P2). Higher-ionization lines of C IV and Si IV may also be detected in some of the objects, but they are even weaker. At these levels, all or most of their equivalent widths may also be interstellar; evidence for truly photospheric stellar lines is tenuous. From detected *absorption* lines, DG 353 has a redshift of $z = 3.9757 \pm 0.0026$ (7 lines), DG 433 has a redshift of $z = 3.3435 \pm 0.0026$ (6 lines), and P1/P2 has a redshift of $z = 3.9752 \pm 0.0039$ (7 lines). The absorption-line redshift of P1/P2 is consistent with that of DG 353. The quoted errors are the RMS errors of the means based on the scatter in all detected absorption lines. Only the Si II–C IV absorption complex is potentially detected in A0; its redshift is consistent with the Ly α redshift, though the region is heavily contaminated by poor subtraction of night-sky emission.

Ly α in emission is detected in all objects except DG 433. From Ly α alone, the formal redshift of DG 353 is $z = 3.9837 \pm 0.0001$, that of P1/P2 is $z = 3.9822 \pm 0.0001$, and that of A0 is $z = 3.9812 \pm 0.0001$ (errors are centering errors only). Note that for DG 353, this Ly α redshift implies a velocity difference with respect to the absorption lines of 480 km s^{-1} in the rest frame of the object; for P1/P2, the implied velocity difference is 420 km s^{-1} . The formal velocity difference between DG 353 and P1/P2 is $\Delta z = 0.0015 \pm 0.0001$, about 80 km s^{-1} in the restframe.

The 15σ formal difference between the Ly α redshifts of DG 353 and P1/P2, which have

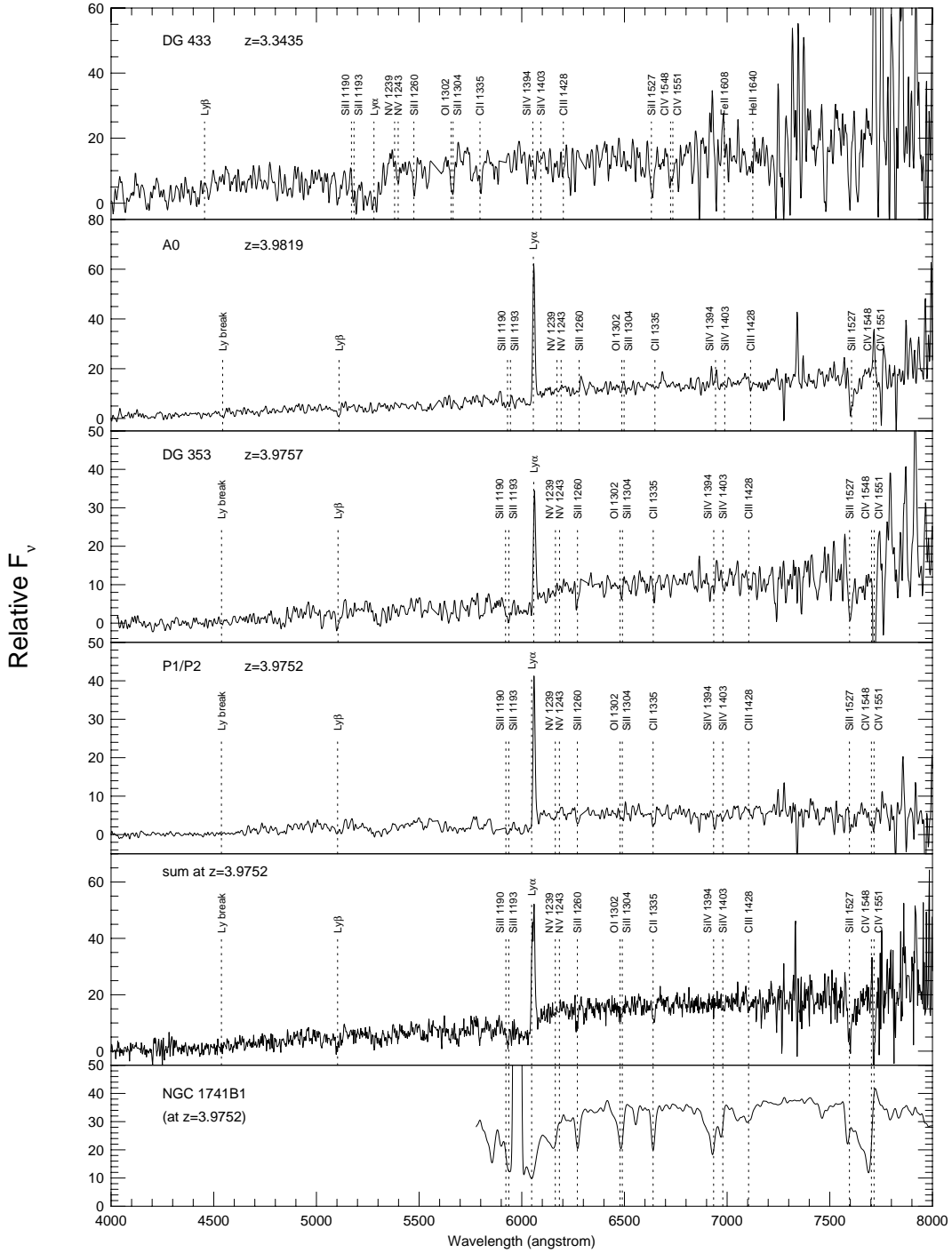


Fig. 2.— Spectra of the four $z > 3$ objects. The fifth panel is a sum of the four objects, corrected to a common redshift. A spectrum of NGC 1741B1 (kindly provided by C. Leitherer), a bright knot in a local starburst, has been redshifted and smoothed to match the object spectra.

Table 1. Object properties.

Name	z_{abs}	$z_{Ly\alpha}$ ^a	R_{702}^{iso} ^b	R_{702}^{Kron} ^c	peak SB ^d (mag/□'')	area (□'')	axial ratio
DG 433	3.3435	...	24.46	23.31	22.28	0.25	0.69
DG 353	3.9757	3.9822 ^f	23.27	22.78	21.76	0.59	0.84
					21.76		
					21.85		
P1/P2	3.9752	3.9822	22.62	22.00	21.39	1.10	0.40
P1					21.39		
P2					21.57		
A0	...	3.9819 ^f	23.58	... ^g	22.13	0.49	0.21 ^h

^aSee Table 2

^bIsophotal magnitude at 23.5 mag/□''

^cElliptical aperture magnitude with semimajor axis as defined by Bertin & Arnouts (1996), following Kron (1980); an approximation to the total magnitude

^dSurface brightness of peak pixel

^eIsophotal area at 23.5 mag/□''

^fAfter correction for a zero-point shift and wavelength scale stretching with respect to P1/P2; see Section 3.2

^gContaminated by neighboring large elliptical DG 367 (Dressler & Gunn 1992)

^hA0 only marginally resolved along short axis

Table 2. Cross-correlation velocity differences.

Name	Name	Δv (km s ⁻¹) Na D λ 5893	Δv (km s ⁻¹) O I λ 6300	Δv (km s ⁻¹) Ly α	Δv_{corr} (km s ⁻¹) Ly α ^a
DG 353	P1/P2	75 ± 4	101 ± 13	80 ± 44	6 ± 45
A0	P1/P2	32 ± 2	40 ± 5	119 ± 44	83 ± 44

^aAfter correction for wavelength zero-point differences and stretchings.

consistent absorption redshifts, appears to be an artifact of the wavelength calibration process. In order to check our wavelength solutions between exposures and runs, we performed cross-correlations of the wavelength-calibrated, rectified spectra before sky-subtraction. Using the RV.FXCOR task in IRAF, we cross-correlated the spectra of DG 353 and P1/P2 in 200Å regions around both the Na D $\lambda 5893$ and O I $\lambda 6300$ night-sky emission lines. The measured velocity differences are $75 \pm 4 \text{ km s}^{-1}$ and $101 \pm 13 \text{ km s}^{-1}$, respectively, indicating a slight wavelength stretch. Cross-correlation of a 100Å region around Ly α at $\approx 6060\text{Å}$ found a velocity difference of $80 \pm 6 \text{ km s}^{-1}$. This error is the formal error from the cross-correlation routine; however, the line profiles are skewed, and we estimate the true uncertainty to be closer to $\pm 44 \text{ km s}^{-1}$, or one-tenth of the FWHM of Ly α in these objects. After correction for both the zero-point difference and wavelength stretching, the velocity difference between the Ly α lines of DG 353 and P1/P2 is only $6 \pm 45 \text{ km s}^{-1}$. The 80 km s^{-1} correction is small compared to the errors of the absorption-line redshifts and does not disturb their previous agreement. The absorption-line redshifts are derived from lines over a broad spectral region, and local wavelength shifts are not important, in contrast to Ly α . P1/P2 and DG 353 thus have consistent absorption-line and emission-line redshifts. Their spectra are also consistent.

We performed a similar cross-correlation analysis on the spectra of P1/P2 and A0 (taken on the same run). The measured velocity differences for Na D $\lambda 5893$ and O I $\lambda 6300$ are $32 \pm 2 \text{ km s}^{-1}$ and $40 \pm 5 \text{ km s}^{-1}$, respectively. Cross-correlation of the Ly α regions determined a velocity difference of $119 \pm 3 \text{ km s}^{-1}$, but the uncertainty is again probably closer to $\pm 44 \text{ km s}^{-1}$. After correction for the difference in wavelength calibrations, the velocity difference between the Ly α lines of A0 and P1/P2 is $83 \pm 44 \text{ km s}^{-1}$, indicating a marginally significant difference. The spectra of these objects are also different; P1/P2 clearly has interstellar absorption lines, while A0 appears to be line-free. Table 2 presents a summary of the velocity differences as determined by cross-correlation.

3.2. Photometry

Isophotal magnitudes and areas were measured from stacked, geometrically-corrected WFPC2 F702W (hereafter called R_{702}) images of Dressler et al. (1994b) using the SExtractor faint-galaxy photometry package (Bertin & Arnouts 1996). Figure 1 shows the core of the cluster, in WF2. Magnitudes were calibrated using the “synthetic” WFPC2 system of Holtzman et al. (1995). The 3σ surface brightness limit in this frame from Poisson noise of the sky is $\approx 25.9 \text{ mag}/\square''$; however, a relatively high surface brightness threshold of $23.5 \text{ mag}/\square''$ was applied, as A0 is blended with the large nearby elliptical DG 367 (Dressler & Gunn 1992) at fainter levels. Elliptical aperture magnitudes approximating total aperture magnitudes were also measured following a modified version of the Kron (1980) r_1 aperture magnitude scheme, as described by Berin & Arnouts (1996). Table 1 summarizes the properties of these four objects, including redshifts, R_{702} isophotal and Kron aperture magnitudes, peak surface brightnesses, isophotal areas, and axial ratios.

4. Gravitational lensing

Seitz et al. (1996) have suggested that P1/P2 and DG 353 are a lensed pair and that A0 is a gravitational arc. The coincident redshifts of P1/P2 and DG 353 and their similar spectra and double-knot morphologies support this suggestion, but more detailed modelling of the cluster potential will be necessary to determine if these objects do indeed share a common source. A0, with its slightly discrepant redshift, line-free spectrum, and smooth morphology, may also be lensed but probably is not another image of the possible source galaxy of P1/P2/DG 353.

DG 433 is far enough outside the cluster core, $35'' = 161 (176) h^{-1}$ kpc [$q_0 = 0.5 (0.05)$] projected distance from the three dominant elliptical galaxies, that it is not expected to be greatly distorted or amplified by the cluster potential. The mean ellipticity expected at the position of DG 433 from Figure 3 of Seitz et al. (1996) is $\|\bar{\epsilon}\| \approx 0.083$. This corresponds to a stretching of about 18% (roughly along the major axis) and a brightening of about 0.18 mag. The HST image of this galaxy is thus more likely to be a truer representation of its ultraviolet morphology than those of the other three objects.

5. Object properties

5.1. Metallicities

As pointed out by Pettini & Lipman (1995) and Steidel et al. (1996a), it is difficult to determine precisely the metallicities of galaxies using low-resolution spectra of far-UV absorption lines. However, one can make a very crude estimate by comparing to the stellar absorption lines in nearby O stars and starburst galaxies. Walborn et al. (1995) note that the high-excitation lines N V, Si IV, and C IV are produced mostly in stellar photospheres, and their strength is an indicator of stellar surface abundance. This is confirmed by comparing UV spectra of O stars from the SMC ($[\text{Fe}/\text{H}] = -0.65$, Russell & Bessell 1989) with similar stars from the LMC ($[\text{Fe}/\text{H}] = -0.30$). N V is occasionally strong in SMC stars, probably due to dredge-up of CNO processed material from the interior (Maeder & Conti 1994), but all three lines would certainly be weak in a composite UV spectrum of the SMC. These features are also uniformly quite strong in the solar-abundance starburst models of Leitherer, Robert, & Heckman (1995).

The fifth panel of Figure 2 shows a composite sum of the four distant galaxy spectra presented here. N V, Si IV, and C IV are all weak or absent. The weakness of C IV is particularly telling. In local O stars and starburst galaxies, it is the most constant and reliable stellar line, and the starburst spectrum of NGC 1741B1 (bottom panel of Figure 2; $[\text{O}/\text{H}] = -0.61$, Vacca & Conti 1992) is an indicator of the expected strength of C IV near solar metallicity. C IV is contaminated by strong sky lines in three of our four objects, but nevertheless it is clear that its strength in the sum is much weaker than in NGC 1741B1. Finally, the near-total lack of *any* line in A0 (including interstellar lines, which are strong in the SMC despite its low metallicity) suggests an *extremely*

low metallicity for this object.

The average stellar line strength of our objects is strikingly similar, or perhaps even weaker, than that of the composite spectrum of 11 high-redshift galaxies shown by Lowenthal et al. (1997). Furthermore, including the spectra of Steidel and collaborators (Steidel et al. 1996a, 1996b), a total of more than 25 galaxies at $z > 2.5$ have been observed so far, yet *not one* has shown stellar line strengths approaching those of the local solar-metallicity starburst NGC 1741. An exact estimate of the metallicities of high-redshift galaxies awaits higher signal-to-noise spectra as well as non-solar-abundance starburst models (Robert et al., in preparation). However, a rough comparison suggests that the average mean metallicity of these objects is at least as low as the SMC, *i.e.*, $Z \lesssim 0.1Z_{\odot}$. Thus, we suggest that high-redshift galaxies as a class are likely to be metal poor.

5.2. Dust

A rough estimate of the reddening of DG 433 and DG 353 can be made by appealing to their ground-based $g - r$ colors: 1.09 and 1.24, respectively (Gunn & Dressler, unpublished; the ground-based colors of P1/P2 and A0 are contaminated by nearby objects). Using unreddened models of very young star-forming galaxies observed at the appropriate redshifts (Bruzual & Charlot 1993; continuous star-forming galaxy models of 10 and 50 Myr kindly provided by C. Gronwall) and taking into account the blanketing of the g band by the Ly α forest calculated by Madau (1995), one expects $g - r \approx 0.1$ and ≈ 0.8 for DG 433 and DG 353, respectively. These colors imply reddenings of $E(g - r) \approx 1.0$ and ≈ 0.4 mag. For a simplified foreground screen model and an SMC extinction law (Calzetti, Kinney, & Storchi-Bergmann 1994) appropriate to low metallicities, these values correspond to extinctions at observed r (rest 1500 Å and 1300 Å, respectively) of 1.9 and 0.9 magnitudes. This corresponds to optical restframe internal reddenings of $E(B - V) = 0.15$ and 0.06 mag. These estimates are rough owing to the use of a foreground screen model and uncertainties in the reddening curve. However, they suggest that the observed UV luminosities may need to be corrected upwards by modest factors (2–6). This amount of UV absorption is adequate to reduce Ly α to the modest levels generally seen in high-redshift galaxies (Charlot & Fall 1993).

5.3. Star Formation Rates

In the absence of large dust extinction, star formation rates can be estimated directly from the rest-frame far-UV flux observed in the *Hubble Space Telescope* images. A ~ 7 Myr old “continuous star formation” model from the evolutionary-synthesis models of Leitherer, Robert, & Heckman (1995) with $Z = Z_{\odot}$ produces a rest-frame luminosity at 1500 Å of $L_{1500} = 10^{40.1}$ erg s $^{-1}$ Å $^{-1}$ (models with $Z = 0.1Z_{\odot}$ have similar continuum luminosities; Robert, private communication).

The effective wavelengths of the F702W filter at $z = 3.35$ and $z = 3.98$ are $\approx 1600 \text{ \AA}$ and $\approx 1400 \text{ \AA}$; to compute L_{1500} , we note that, redwards of $\text{Ly}\alpha$, $f_\lambda \propto \lambda^{-2}$ for DG 433, P1/P2, and DG 353, and $f_\lambda \propto \lambda^{-2.5}$ for A0. The isophotal F702W magnitudes R_{702}^{iso} (Column 4 of Table 2) imply raw star formation rates, ignoring possible gravitational lensing, of $2.5 (7.8) h^{-2} M_\odot \text{ yr}^{-1}$ (DG 433), $7.1 (25.) h^{-2} M_\odot \text{ yr}^{-1}$ (A0), $18. (63.) h^{-2} M_\odot \text{ yr}^{-1}$ (P1/P2), and $9.8 (31.) h^{-2} M_\odot \text{ yr}^{-1}$ (DG 353) for $q_0 = 0.5$ ($q_0 = 0.05$). Correcting for the possible weak-field lensing of DG 433 mentioned above would reduce its star formation rate to $2.1 (6.6) h^{-2} M_\odot \text{ yr}^{-1}$, and the star formation rates of A0, P1/P2 and DG 353 are upper limits in the absence of a lensing correction. Accounting for extinction in DG 433 would raise its SFR to $12. (38.) h^{-2} M_\odot \text{ yr}^{-1}$, including the weak-field lensing; for DG 353, accounting for extinction would raise its SFR to $22. (78.) h^{-2} M_\odot \text{ yr}^{-1}$, ignoring any lensing.

To summarize, an average *raw* star formation rate of $9.3 (32.) h^{-2} M_\odot \text{ yr}^{-1}$, plus an average correction factor of ~ 4 for extinction, yields a corrected average rate of $\approx 32. (120.) h^{-2} M_\odot \text{ yr}^{-1}$. The raw rate is higher than the average raw star formation rate measured by Lowenthal et al. (1997), $\dot{M} = 1.7 (4.7) h^{-2} M_\odot \text{ yr}^{-1}$ based on 11 galaxies. However, three of the four objects here may be significantly lensed, and their inferred star formation rates are therefore upper limits.

Sizes of these objects are difficult to measure due to possible lensing, but the raw half-light radii are $\lesssim 0''.5$, corresponding to $\lesssim 8. (15.) h^{-1} \text{ kpc}$ for $q_0 = 0.5 (0.05)$. These are comparable to the radii seen among other high-redshift objects (Giavalisco, Steidel, & Macchetto 1996; Lowenthal et al. 1997).

6. Implications

From a handful of early studies, a portrait of high-redshift “normal” galaxies is beginning to emerge (Steidel et al. 1996a, 1996b; Giavalisco, Steidel, & Macchetto 1996; Lowenthal et al. 1997). They have star-formation rates of $1\text{--}10 h^{-2} M_\odot \text{ yr}^{-1}$, rest frame B -band luminosities of $1\text{--}\text{few } L^*$, and half-light radii of $1\text{--}10 \text{ kpc}$. Morphologically, they usually consist of compact, high-surface-brightness blobs, typically single, sometimes multiple, and sometimes imbedded in lower-surface-brightness, diffuse luminosity. The co-moving number density of high-redshift galaxies now approaches or exceeds the local number density of $L > L^*$ galaxies (Lowenthal et al. 1997).

What kind of local objects will these high-redshift galaxies evolve into, and what kind of snapshot of early galaxy formation do they provide? Steidel et al. (1996a, 1996b) and Giavalisco et al. (1996) have suggested that they may represent the *cores* of future massive spheroids. They cite the smooth, compact morphologies of their sample, plus a tentative estimate of virial motions $\sim 200 \text{ km s}^{-1}$ based on the equivalent widths of interstellar absorption lines. As the lookback time to $z = 3.5$ is $13.5 (12.5) \text{ Gyr}$ for $t_0 = 15 \text{ Gyr}$ and $q_0 = 0.5 (0.05)$, the stars in high-redshift galaxies are plausibly identified with local old spheroid populations. Finally, the presence of compact,

sometimes multiple blobs and diffuse emission indicates that the stars that have already formed will not ultimately reside in flattened, rotating disks. Either the blobs will remain isolated or they will merge with other blobs. In either, case the stars that we now see will populate a spheroidal density distribution, strengthening the identification with local spheroids.

Despite these parallels, further data suggest that the massive core hypothesis may need some revision. First, the equivalent widths of the interstellar lines have been challenged as indicators of internal, gravitational motions (Conti, Leitherer & Vacca 1996)—saturation effects are just too uncertain. It seems fair to say that the internal motions of high-redshift galaxies are presently unknown—these galaxies could be massive or not. Second, strong redshift clustering has not been detected for the high-redshift population (Lowenthal et al. 1997; Steidel et al. 1996a), except possibly in the fields of QSOs (Malkan, Teplitz & McLean 1996; Hu, McMahon, & Egami 1996; Hu & McMahon 1996). The high-redshift population is thus likely to be a *field* population, not the precursor of clusters. This, together with the large number density approaching or exceeding the local value of $N(L > L^*)$, suggests that these objects are not the precursors of *ellipticals* but rather the spheroids of early-type (mostly field) *spirals*, which are locally much more numerous than ellipticals.

Equating high-redshift galaxies with local spheroids rather than massive ellipticals goes some way towards solving a size discrepancy that results from the latter hypothesis. A massive elliptical like M87 would have an apparent half-light radius $\approx 0.9 h$ (for $q_0 = 0.5$ and an age of 1 Gyr) at $z = 3$. This is five to ten times larger than the typical half-light radii of the compact high-redshift blobs, which are more consistent with those of local bulges (Bender, Burstein, & Faber 1992, as noted by Lowenthal et al. 1997).

However, this seeming agreement conceals a serious problem, as Lowenthal et al. (1997) note. The observation that the stars of high-redshift galaxies are *metal-poor* suggests that we should properly be comparing high-redshift radii to the radii of the metal-poor (*i.e.*, Population II) components of local spheroids. These are larger than the half-light radii given above—in the Milky Way, for example, the halo globular cluster population with $Z < 0.1Z_\odot$ has a mean radius of 10 kpc (Harris & Racine 1979) and extends to ~ 50 kpc. These are also much larger than the typical spheroid half-light radius $r_{1/2} \sim 2$ kpc (Bender, Burstein, & Faber 1992). The half-light radius of the Population II field stars in the Milky Way is not known, but since the bulge of the Galaxy is metal-rich (McWilliam & Rich 1994; Sadler, Rich, & Terndrup 1996), there can be no doubt that r_e for the metal-poor stars is much larger than r_e for the bulge. The identification of high-redshift stars with local metal-poor Population II components tends to reintroduce the size discrepancy.

We suggest that the resolution of this discrepancy may be found in the currently popular theory for the formation of spheroids via hierarchical clustering and merging. Hierarchical clustering predicts that highly overdense systems like those believed to form spheroids and bulges begin to collapse with many subclumps (Blumenthal et al. 1984). Searle & Zinn (1978) presented a subclump formation model of the metal-poor spheroid of the Milky Way that in many respects

is similar. The essence of these pictures is that the first (metal-poor) stars are formed in small clumps distributed *throughout* the volume that will later become the Population II spheroid. As these clumps merge, they create a large, diffuse halo of metal-poor stars. Meanwhile, enriched gas continues to dissipate and fall to the center of the global potential well, giving rise to successive generations of more metal-rich and more centrally concentrated stars. This is essentially a clumpy version of the collapse picture for the Milky Way spheroid advocated by Eggen, Lynden-Bell, & Sandage (1962) and seen now in more realistic hydrodynamic simulations (*e.g.*, Steinmetz & Muller 1995). Thus, spheroids do not form from the inside out, as massive cores accreting matter to well-defined centers, but from the outside in, with the first stars more widely distributed than the later ones. We suggest that the compact blobs of the high-redshift galaxies should be equated with the subclumps of the Searle-Zinn and hierarchical clustering models. In that case, their small radii pose no contradiction. This interpretation was first put forward as one of several scenarios by Lowenthal et al. (1997).

The high co-moving number density of high-redshift galaxies is comparable to the local co-moving number density of spheroids (Lowenthal et al. 1997). If the above identification with local spheroids is correct, this implies that we are seeing roughly *all* forming spheroids at high-redshift. In other words, the structure in and around the luminous blobs must be a statistically representative snapshot of what an early spheroid looked like. Given the present size of the Population II component in the Milky Way, we might therefore expect to see a *population* of subclumps in every high-redshift spheroid, distributed over a volume $\gtrsim 20$ kpc in diameter, or $\gtrsim 1''.4$ ($0''.8$) on the sky for $q_0 = 0.5$ (0.05). We do not see that. Instead, we see most often only one blob, or at most a few blobs, in a significantly smaller volume. There are a handful of cases (Lowenthal et al. 1997; Giavalisco, Steidel, & Macchetto 1996) where companion blobs separated by $\sim 1''$ have colors that suggest similar redshifts, but it seems possible that there are few *large populations* of bright blobs filling such volumes.

This contradiction might be resolved if each individual blob was bright for a short time, so that, on average, *only one blob is seen at a time*. We would then have a “Christmas tree” model (Lowenthal et al. 1997), wherein small individual star-forming blobs come and go within a much larger and largely invisible spheroid structure. Semi-analytic models of galaxy formation (Somerville & Primack, priv. comm.) currently do not make blobs nearly as bright as the $z > 3$ galaxies seen. However, these authors have suggested that allowing blobs to collide with each other, triggering star formation, might produce blobs occasionally bright enough to reproduce the $z > 3$ galaxies observed.

Alternatively, dust could hide blobs. Every spectroscopically-confirmed $z > 3$ galaxy to date has very weak stellar absorption-line features suggesting low metallicity. If dust content were to increase with metallicity, clumps might *self-obscure* as star-formation and nucleosynthesis proceeded (Charlot & Fall 1993). If this process were rapid, only a few blobs might be seen at a time.

We may now enquire whether either of these models is consistent with known constraints on the timescale of spheroid formation. Let n_v be the number of blobs visible at any given time, and let t_v be the time a blob is visible. Let N_b be the total number of blobs needed to form a spheroid of mass M_S over total time T_S . Then

$$n_v = \frac{t_v N_b}{T_S}. \quad (1)$$

If t_* is the star-formation timescale of a blob, the quantity

$$f = \frac{t_v}{t_*} \leq 1 \quad (2)$$

is the fraction of time that a blob is visible while forming stars. If M_b is a typical blob stellar mass and R is its star-formation rate, then

$$N_b M_b = M_S, \quad M_b = R t_* \quad (3)$$

and the number of blobs visible at any one time is

$$n_b = f \frac{M_S}{R T_S}. \quad (4)$$

Thus, if $n_b \approx 1$ as observed and $f = 1$, the timescale for forming a $10^{10} M_\odot$ spheroid is

$$T_s \approx \begin{array}{l} 3 \times 10^9 \text{ yr} \\ 3 \times 10^8 \text{ yr} \end{array} \quad \text{for } R = \begin{array}{l} 3 M_\odot \text{ yr}^{-1} \\ 30 M_\odot \text{ yr}^{-1} \end{array}. \quad (5)$$

For $f = 0.1$, the timescale for forming a $10^{10} M_\odot$ spheroid is

$$T_s \approx \begin{array}{l} 3 \times 10^8 \text{ yr} \\ 3 \times 10^7 \text{ yr} \end{array} \quad \text{for } R = \begin{array}{l} 3 M_\odot \text{ yr}^{-1} \\ 30 M_\odot \text{ yr}^{-1} \end{array}. \quad (6)$$

The observed star formation rate for the blobs is $R \sim 10 M_\odot \text{ yr}^{-1}$, and an estimated T_S for the Milky Way is $\gtrsim 2 \text{ Gyr}$ (Schuster et al. 1996). These seem more consistent with $f = 1$ than $f = 0.1$. Thus, blobs may not self-obscure due to dust, at least not at very early epochs.

Constraints on blob lifetimes are loose. If blobs make stars only in short bursts, t_* could be as short as the minimum starburst age of $\lesssim 10 \text{ Myr}$, the typical blob stellar mass M_b would be only $\sim 10^8 M_\odot$ for $R = 10 M_\odot \text{ yr}^{-1}$, and there would be 100 blobs per $10^{10} M_\odot$ spheroid. If $t_* = 10^9 \text{ yr}$ (a plausible upper limit), then the blob mass is $10^{10} M_\odot$ and there is only one blob per spheroid. This would be incompatible with the need for collisions among blobs to create an extended Population II halo (Somerville & Primack, priv. comm.). Thus t_* is most likely in the range 10^7 – 10^8 yr . The difference corresponds to a factor of ~ 10 in M/L ratio (Bruzual & Charlot 1993) and might be detectable if linewidths (and masses) could be measured. A longer t_* might also give rise to an older stellar population detectable in the K -band.

7. Summary

We have presented spectra of four objects at $z > 3$, three of which are at $z \approx 4$. These galaxies are

- small: $r_{1/2} \approx 10$ kpc;
- bright: $L_B \sim 1\text{--}10 L_B^*$;
- lumpy, with no more than a few blobs per object;
- likely metal-poor, with $Z \lesssim 0.1Z_\odot$;
- mildly dusty: $E(B - V)_{\text{int}} \lesssim 0.15$;
- and star forming: $\dot{M} \sim 2\text{--}60 M_\odot \text{ yr}^{-1}$.

These particular galaxies probably have been magnified and brightened somewhat by gravitational lensing but otherwise seem to be the higher-redshift analogs of $z \sim 3$ galaxies seen previously (Steidel et al. 1996a, 1996b; Lowenthal et al. 1997). Considering their properties together with the properties of other galaxies at $z > 3$, particularly their metallicities, number density, star-formation rates, and sizes, we suggest that these objects will evolve into the analogs of spheroids, in particular the *Population II components of early-type spirals*. The individual blobs may be identified with the Searle & Zinn (1978) subclumps thought to have formed the Milky Way halo. We present a toy model of the formation of spheroids, with particular emphasis on the number of star-forming blobs visible in a given halo at any one time. Kinematic data on blob masses could be very helpful in testing this “Christmas tree” model.

We thank C. Grillmair and the CARA staff, particularly T. Bida, J. Aycock, and W. Wack, for observing assistance, D. Kelson and A. Phillips for software and support, C. Leitherer for providing the spectrum of NGC 1741B1, C. Gronwall and P. Madau for providing digital versions of model data, C. Robert for providing models in advance of publication, I. Smail, J.-P. Kneib, C. Steidel, M. Giavalisco, J. Lowenthal, E. Groth, and E. Shaya for helpful discussions, and an anonymous referee for comments that substantially improved the manuscript. This work was partially supported by a Flintridge Fellowship to SCT and by NASA contract NAS5-1661 to the WF/PC-I IDT.

REFERENCES

- Bender, R., Burstein, D., & Faber, S. M. 1992, *ApJ*, 399, 462
- Bertin, E. & Arnouts, S. 1996, *A&AS*, 117, 393
- Blumenthal, G. R., Faber, S. M., Primack, J. R., & Rees, M. J. 1984, *Nature*, 311, 517
- Bruzual, G. & Charlot, S. 1993, *ApJ*, 405, 538
- Calzetti, D., Kinney, A. L., Storchi-Bergmann, T. 1994, *ApJ*, 429, 582
- Charlot, S. & Fall, S. M. 1993, *ApJ*, 415, 580
- Conti, P. S., Leitherer, C., & Vacca, W. D. 1996, *ApJ*, 461, L87
- Dressler, A. & Gunn, J. E. 1992, *ApJS*, 78, 1
- Dressler, A., Oemler, A., Butcher, H., & Gunn, J. E. 1993, *ApJ*, 404, L45
- Dressler, A., Oemler, A., Butcher, H., & Gunn, J. E. 1994a, *ApJ*, 430, 107
- Dressler, A., Oemler, A., Sparks, W. B., & Lucas, R. A. 1994b, *ApJ*, 435, L23
- Ebbels, T. M. D., Le Borgne, J.-F., Pelló, R., Ellis, R.S., Kneib, J.-P., Smail, I., & Sanahuja, B. 1996, *MNRAS*, 281, L75
- Eggen, O. J., Lynden-Bell, D., & Sandage, A. 1962, *ApJ*, 136, 748
- Ellingson, E., Yee, H. K. C., Bechtold, J., & Elston, R. 1996, *ApJ*, 466, L71
- Fukugita, M., Shimasaku, K., & Ichikawa, T. 1995, *PASP*, 107, 945
- Giavalisco, M., Steidel, C. C., & Macchetto, D. F. 1996, *ApJ*, 470, 189
- Harris, W. E. & Racine, R. 1979, *ARA&A*, 17, 241
- Holtzman, J. A., Burrows, C. J., Casertano, S., Hester, J. J., Watson, A. M., & Worthey, G. 1995, *PASP*, 107, 1065
- Hu, E. M., McMahon, R. G., & Egami, E. 1996, *ApJ*, 459, L53
- Hu, E. M. & McMahon, R. G. 1996, *Nature*, 382, 231
- Kelson, D. D., van Dokkum, P., Franx, M., Illingworth, G. D. 1997, in preparation
- Kron, R. G. 1980, *ApJS*, 43, 305
- Leitherer, C., Robert, C., & Heckman, T. M. 1995, *ApJS*, 99, 173

- Lowenthal, J. D., Guzmán, R., Gallego, J., Koo, D. C., Phillips, A. C., Vogt, N. P., Faber, S. M., Illingworth, G. D., Gronwall, C. 1997, *ApJ*, in press
- Madau, P. 1995, *ApJ*, 441, 18
- Maeder, A. & Conti, P. S. 1994, *ARA&A*, 32, 227
- Malkan, M. A., Teplitz, H., & McLean, I. S. 1996, *ApJ*, 468, L9
- McWilliam, A. & Rich, R. M. 1994, *ApJS*, 91, 749
- Moore, B., Katz, N., Lake, G., Dressler, A., & Oemler, A. 1996, *Nature*, 379, 613
- Oke, J. B., et al. 1995, *PASP*, 107, 375
- Petitjean, P., Pécontal, E., Valls-Gabaud, D., & Charlot, S. 1996, *Nature*, 380, 411
- Pettini, M. & Lipman, K. 1995, *A&A*, 297, L63
- Russell, S. C. & Bessell, M. S. 1989, *ApJS*, 70, 865
- Sadler, E. M., Rich, R. M., & Terndrup, D. M. 1996, *AJ*, 112, 171
- Searle, L. & Zinn, R. 1978, *ApJ*, 225, 357
- Schuster, W. J., Nissem, P. E., Parrao, L., Beers, T. C., & Overgaard, L. P. 1996, *A&AS*, 117, 317
- Seitz, C., Kneib, J.-P., Schneider, P. & Seitz, S. 1996, *A&A*, 314, 707
- Steidel, C. C., Giavalisco, M., Pettini, M., Dickinson, M., & Adelberger, K. L. 1996a, *ApJ*, 462, L17
- Steidel, C. C., Giavalisco, M., Dickinson, M., & Adelberger, K. L. 1996b, *AJ*, 112, 352
- Steinmetz, M. & Muller E. *MNRAS*, 276, 549
- Trager, S. C. 1997, Ph.D. Thesis, UC Santa Cruz
- Vacca, W. D. & Conti, P. S. 1992, *ApJ*, 401, 543
- Walborn, N. R., Lennon, D. J., Haser, S. M., Kudritzki, R.-P., & Voels, S. A. 1995, *PASP*, 107, 104
- Yee, H. K. C., Ellingson, E., Bechtold, J., Carlberg, R. G., & Cuillandre, J.-C. 1996, *AJ*, 111, 1783